Potential Energy Power from Tidal Current in Lagoon System – The Case of Oualidia Lagoon, Morocco

8 authors, including:

Mohammed Bouchkara
Institut National de Recherche Halieutique
16 PUBLICATIONS **8** CITATIONS

SEE PROFILE

Hendry Siagian
Universitas Diponegoro
26 PUBLICATIONS **77** CITATIONS

SEE PROFILE

Nouhaila Erraji Chahid
Université Chouaib Doukkali
9 PUBLICATIONS **3** CITATIONS

SEE PROFILE

Imane Joudar
Université Chouaib Doukkali
8 PUBLICATIONS **3** CITATIONS

SEE PROFILE

Potential Energy Power from Tidal Current in Lagoon System – The Case of Oualidia Lagoon, Morocco

Mohammed Bouchkara[1*], Hendry Siagian[2], Nouhaila Erraji Chahid[1], Imane Joudar[1], Charaf Hajjaj[3], Aïssa Benazzouz[4], Bendahhou Zourarah[1], Khalid El Khalidi[1]

[1] Marine Geosciences and Soil Science Laboratory (URAC-45), Earth Sciences Department, Faculty of Sciences, Chouaib Doukkali University, Av. des Facultés, El Jadida 24000, Morocco

[2] Departement of Oceanography, Faculty of Fisheries and Marine Science, Diponegoro University, Jl. Prof. Sudarto No. 13, Tembalang, Kec. Tembalang, Kota Semarang, Java Tengah 50275, Indonesia

[3] Highet School of Technology [ESTE], Cadi Ayyad University, Km 9, Route d'Agadir, Essaouira Aljadida BP. 383, Ghazoua, Essaouira 44000, Morocco

[4] Nautical Science and Naval Engineering Department, Institut Supérieur d'Etudes Maritimes, Km 7, Road El Jadida, Casablanca B.P. 20520, Morocco

* Corresponding author's e-mail: m.bouchkara@yahoo.com

ABSTRACT

The lagoon is a natural system protected from the sea by a dune barrier creating energy from the movement of rising and falling tides, thus providing a sustainable option for extracting energy from tidal currents. The energy that can be extracted is one of the most potential renewable energy sources. Therefore, the interaction of tidal currents with stratification layers has become important to optimize the efficiency of energy conversion at each depth layer in water masses. We have chosen as a case study, the Oualidia lagoon (Atlantic coast of Morocco). This ecosystem is characterized by hydrodynamics relatively favored by tides and tidal currents which are the main intra-lagoon currents, with a predominance of the semi-diurnal component M2 (period of 12 h 25) with 2.1 to 3.4 m of tidal range. The Multicell Argonaut-XR ADCP is used to measure the current velocity in the Oualidia lagoon at three different stations to study tidal patterns in a vertical layer of water depth. At each station, current velocities were recorded in each 0.5 m layer over a depth of about 5 m. As a result, this study showed that current velocity measurements to be used as renewable energy are found at station 1 located at a depth of 3.5 meters (~layer 5) with a current velocity of 0.771 m/s and a power density value of 235.344 W/m², station 2 located at a depth of 3.5 meters (~layer 5) with a current velocity of 0.4 m/s and a power density value of 32.86 W/m² and station 3 is located at a depth of 3 meters (~layer 6) with a current velocity of 0.527 m/s and a power density value of 75.157 W/m². The variation in current velocities between the different stations is mainly influenced by tides (Flood/ebb), the period of the measurements and the location of the stations. This work presents a model for extracting electrical energy through the use of tidal and current flow variations in such semi-enclosed natural system including lagoons.

Keywords: tidal current, ADCP, power density, marine energy.

INTRODUCTION

The oceans, which cover 70% of our planet, constitute the largest energy reserve in the world. That is why a strong focus on marine renewable energy (MRE), in particular marine current energy (MCE), has been shown by several communities such as the United Kingdom (Blunden and Bahaj, 2006; Serhadlıoğlu et al., 2013), Iran (Abbaspour and Rahimi, 2011), France (Guillou et al., 2018), Mexico (Mejia-Olivares et al., 2018), Canada (Cornett et al., 2010).

Today, There are four types of green energy based on ocean renewable energy that are becoming promising for future use: wave energy, tidal energy, ocean thermal energy, and ocean current

energy (Natalia Moreno et. al., 2010). Ocean tidal current energy resources have many advantages over other renewable energy resources, they are characterized by their predictability over a long period (Ferro, 2006), the density of seawater is higher than that of air, there is 800 x greater density than the wind (Kiho, 2011), (Garcia Novo and Kyozuka, 2016), and they have no environmental impact (Ferro, 2006). As defined, ocean currents are the ongoing flow of water in the ocean in specific directions. Also, the tidal current is a predictable phenomenon produced by the interaction of gravitational forces between the sun, the moon, and the rotation of the earth. It is influenced by many parameters such as salinity, temperature, and sea level (Rourke et al., 2010). However, tidal currents can vary considerably in terms of dominant driving forces, spatial locations, spatial-temporal scales and vertically distribution of physical parameters in water bodies including tidal currents. Consequently, the knowledge of the distribution velocities of the tidal currents is an important task for the evaluation of its potential as well as for the adequate selection of the site to implement the recovery system.

Morocco, situated in the northwest of Africa, knowing by its two maritime borders with predictable and reliable marine currents of a total length equivalent to 3500 km (Aroussy et al., 2016). This makes Morocco a country with excellent potential in terms marine renewable energy. In the last decades, the energy demand has been increasing in Morocco, due to the high growth in electricity requirements of 6.9% per year (L'Electricité, 2020). In order to satisfy this massive energy requirement, the Moroccan government has released the Renewable Energy Sector Support Law. The recent legislation has included many provisions for the national strategy to develop the sector of renewable energy to cover 20% of the national energy demand for households (MFEMEE, 2012). A recent survey by Morocco's Economic, Social and Environmental Council (EESC) predicts that the country has the potential to generate 96% of its electricity from renewable energy by 2050.

Taking into account the potential of neighboring areas, tidal current energy could be a good alternative to reduce Morocco's dependence on fossil fuels and contribute to the reduction of greenhouse gases (Sierra et al., 2013). In addition to energy production, wave farms can be used for coastal protection to limit erosion processes (Iglesias and Carballo, 2014; Rusu and Onea, 2015).

In order to investigate ways to harness tidal currents, the Moroccan government initiated in January 2021 a roadmap for the development of ocean current energy, which includes ocean current energy, either tidal energy or ocean wave energy. The International Renewable Energy Agency (IRENA) expects that the global installed capacity of offshore wind and ocean energy will reach 228 GW and 10 GW respectively by 2030.

This paper focuses on the description of tidal lagoons, given their potential impact on the local energy system. We chose the Oualidia lagoon (Atlantic coast of Morocco) as a case study in order to evaluate the current velocity and power density capacity at each layer of water depth in different measured stations. For this purpose, Acoustic Doppler Current Profiler (ADCP) was used as a measuring instrument in the lagoon of Oualidia (Atlantic coast of Morocco) to obtain the required current profile. The characteristics of the velocity profile collected by the ADCP were examined for all depth layers of the tidal current energy potential at three stations along the lagoon.

MATERIALS AND METHODS

Study area

The Oualidia lagoon is located on the Atlantic coast of Morocco (32° 44'.42 N – 9° 02'.50 W) (Figure 1). It is characterized by a warm temperate climate and average rainfall, which varies according to fluctuations in the natural rainfall regime. Communication with the ocean is provided by three entrance inlets (Bouchkara et al., 2022). It runs parallel to the coast for a distance of about 7 km. Oualidia lagoon is characterized by hydrodynamics relatively favored by swell and tidal currents which are the main intra-lagoon currents (El Khalidi et al., 2011), with a predominance of the semi-diurnal component M2 (period of 12 h 25) with 2.1 to 3.4 m of tidal range. The average speed of the currents, measured at the inlet of the lagoon in 2002, is relatively high (0.5 to 1 m/s) (Geme, 2003). In addition, during spring tide periods, the maximum velocity is about 0.77 m/s, the flooding time of the tide is 7 h 25 min and the ebb tide is also 5 h during ebb (Hilmi et al., 2005).

The renewal time of the waters of the Oualidia lagoon is an important parameter in understanding its hydrodynamic functioning as reported in (Koutitonsky et al., 2007). It was found that the
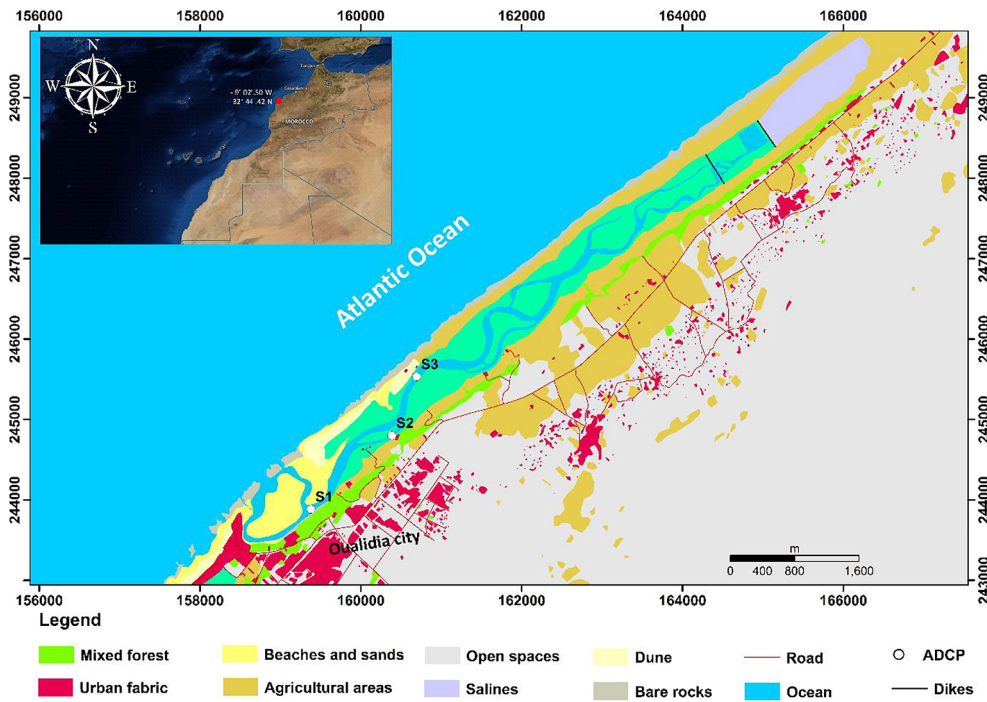
Figure 1. Map showing the study area location and the measured stations (S1, S2, S3) by ADCP

local renewal time (LRT) of the Oualidia lagoon varies between 1 day near the lagoon's entrance inlets to 30 days at its artificial downstream dike and the integral renewal time (IRR) is 15 days on average. The temperature and salinity in this lagoon indicate a clear influence of the marine waters in the downstream zone of the lagoon and a decrease in salinity to the upstream part, due to the presence of numerous freshwater resurgences in the lagoon in permanent activities (Hilmi et al., 2017).

ADCP multicell Argonaut-XR

Current data collection at the Oualidia lagoon has been done using the ADCP Argonaut SonTek XR with a beam sensor wavelength of MHz and an autonomous multicell system (Ismanto et al., 2019). The accuracy of this measurement module is 0.01 m/s, with a maximum column depth of 40 m, a maximum number of cells that can be measured is 10 and a minimum layer thickness of 0.8 m with a maximum speed that can be recorded measuring 6 m/s (Cowles et al., 2017; Ren et al., 2015; Togneri et al., 2017). This equipment has used an acoustic system, by firing a number of sound waves with a 1.5 MHz, and receiving reflected waves of particles moving in the water column, the algorithm interprets as a change in position on the approach of the Doppler effect. We have programmed this ADCP within dynamic column metering mode (XR), In

addition, we use the bottom mounting method on the bottom of the water, in order to get a fixed current velocity (Figure 3). The configurations that we provide for the three stations are presented in the table column below (Table 1).

ADCP measurements were recorded at three different stations in the lagoon (Figure 1), which were used to calculate the characteristics of the vertical velocity profiles, for estimating the power density of each layer vertically. Velocities were recorded at each 0.5 m layer (~10 layers depth), with layer 10 located closest to the water surface, while layer 1 is directly above the ADCP, as shown in Figure 3, from 0.5 m to 5 m above the bottom. The deployment depth was 5 m and data were recorded every 600 s. Presentation of data will be presented in graphic images to describe the results obtained; some of the graphs that will be displayed include line curve graphs, profile graphs, cross sections.

Measurements were carried out at 3 different stations, having continuous temporal variations, station 2 was measured during the neap, then station 3 during the daily neap, and station 1 during the spring (Fig. 2).

Calculation of power density

Utilization of current speed as a source of power density has same principle as wind energy. Compared to wind turbine, ocean current turbine

Table 1. Configuration of measuring speed, current direction, and water level elevation (ADCP)

Module: ADCP SonTek Argonaut-XR frequency, 1,5 Mhz set,	
Configuration	Station measurement set
Station No.	Deployment Date
Station 2	08/04/2021–11/04/2021 (72 h)
Station 3	11/04/2021–14/04/2021 (72 h)
Station 1	14/04/2021–17/04/2021 (72 h)
Duration (h)	3 x 24 h
Deployment depth (m)	6 m
Depth measurement (m)	5.5 m
Vertical layer size/bin (m)	0.5 m
Total layers (m)	10 layers
Interval time sampling (s)	0 – 600 s
Blank distance (m)	0.5 m
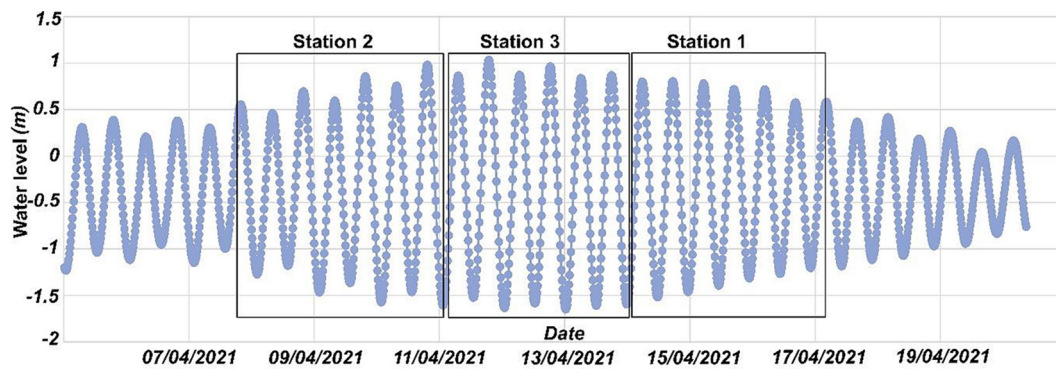
Figure 2. Water level conditions during the period of measurements
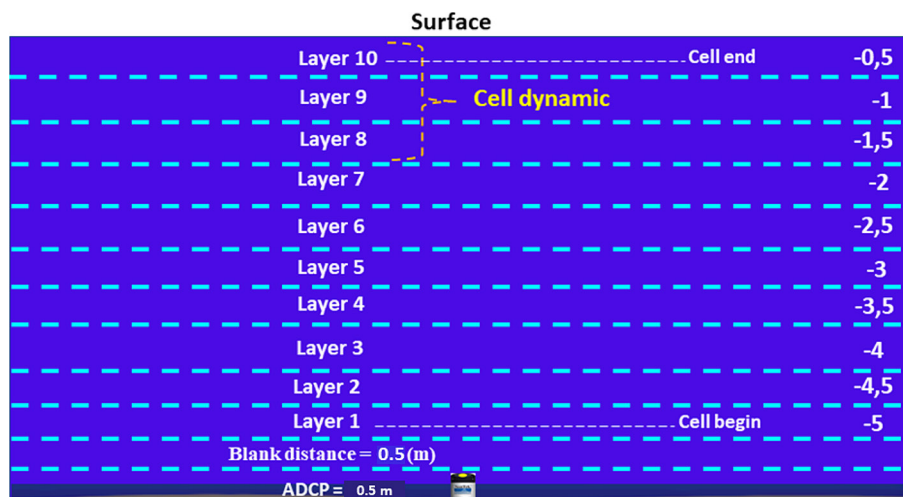
Figure 3. ADCP depth layer profile. Velocities were recorded at each 0.5 m layer (~10 depth layers), layer 10 is located closest to the water surface, while layer 1 (~-5 m) is directly above the ADCP

will produce greater energy, depending seawater has density higher than of air (Hagerman and Polagye, 2006). To examine the temporal variability in available current speed during measurement at each location, mean power during ADCP measurement was calculated based on power density conversion from current speed. The power density is calculated for all depth layer, where P is
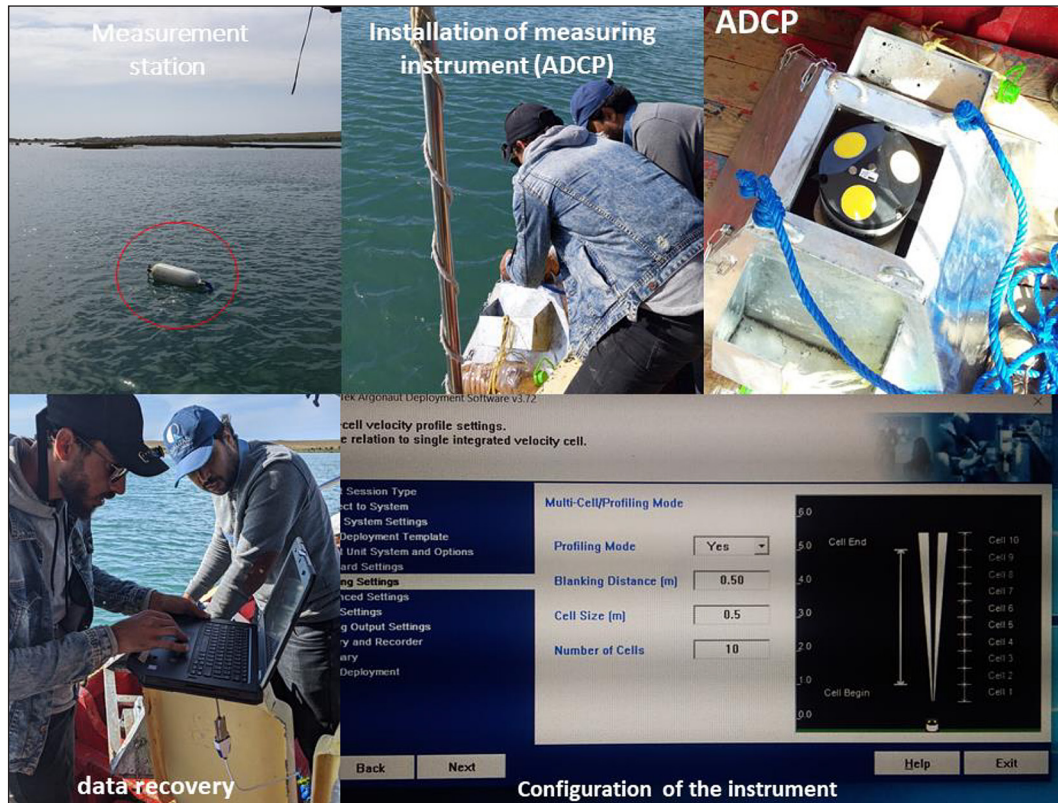
Figure 4. Photos showing the installation and recovery steps of the ADCP instrument

power divided by an area of square (P/A). It equal to the current speed multiplied density of water, we used 1025 kg/m^3 for seawater density (Siagian et al., 2019b).

$$\frac{P}{A} = \frac{1}{2}\rho(u)^3 \qquad (1)$$

In our study, we did not consider the efficiency of the turbine, since we wanted to evaluate the amount of energy for tidal current that can be converted into power density during direct measurements.

RESULTS AND DISCUSSIONS

Tidal current velocity and profile distribution of each layer

The results of the current velocity at the three measurement stations are described and investigated. Current velocity is shown vertically to be able to identify variations in current velocities at each depth (Siagian et al., 2021). A vertical graph is displayed below the Low Astronomical Tide (LAT) value, to present significant results for changes in water (Pu et al., 2017; Siagian et al., 2019a). Station 1 has a maximum current speed of 1.047 m/s with an average speed of 0.550 m/s at layer 6 (-3 m depth). Station 2 has a maximum current speed of 0.644 m/s, with an average speed of 0.308 m/s at layer 8. The current velocity at station 3 is 1.113 m/s with an average current speed of 0.256 m/s, located in the layer 10 (-1 m depth). The average current velocity at the bottom layer sequentially at stations 1, 2, and 3 is 0.46 m/s, 0.284 m/s and 0.304 m/s with the highest maximum speed of 0.89 m/s at station 1.

Based on these results, it is shown on Figure 5 that the current velocity stratification does not occur with the current velocity distribution trend getting stronger at the time of the surface layer. Station 1 has the highest average speed of 0.580 m/s in layer 7, but the maximum speed of layer 7 has decreased by stratification by 0.046 m/s. Station 2 has a maximum speed on the vertical profile at layer 8 with a depth of ~1 m. The average value of the highest current velocity at station 2 is found in layer 5 with a speed of 0.330 m/s. Station 3 has the highest average speed of 0.304 m/s^{-1} at the bottom layer of the waters (Table 2).

The current velocity profile for each station at each depth of the surface waters does not show a distribution trend of increasing velocity. Based on the three stations observed, Station 2 has a smaller current velocity of 0.01 m/s at the surface compared to layer 8. Station 3 has a different trend, with an increasing current velocity in

Table 2. Current velocities measured by ADCP at 3 different stations, in statistical analysis and ten layers of depth

Depth layer profile No.	Water depth layer (m)	Station 2		Station 3		Station 1	
		Current speed (m/s)					
		Averaged	Maximum	Averaged	Maximum	Averaged	Maximum
1	-5.5	0.284	0.597	0.304	0.776	0.460	0.890
2	-5	0.305	0.612	0.296	0.952	0.510	0.960
3	-4.5	0.321	0.613	0.293	0.846	0.540	0.986
4	-4	0.329	0.626	0.276	0.864	0.541	1.033
5	-3.5	0.330	0.62	0.275	0.877	0.544	1.040
6	-3	0.320	0.616	0.297	0.868	0.550	1.047
7	-2.5	0.310	0.627	0.280	0.904	0.580	1.001
8	-2	0.308	0.644	0.271	0.925	0.479	0.930
9	-1.5	0.278	0.643	0.255	1.050	0.390	0.860
10	-1	0.229	0.631	0.256	1.113	0.310	0.760

the layer near the surface of 0.197 m/s. The results of vertical profiling have helped us in determining the layer that can be studied in the utilization of current to be converted into energy. The current velocity parameter is directly proportional to the power density to be generated (Hagerman and Polagye, 2006; Siagian et al., 2019b, 2019a). The optimal layer that can be utilized in the conversion of current to power density is a layer that has connection stability between the average and maximum current velocity values at that depth (Neill et al., 2018). Based on the three stations, layers 4, 5, and 6 have stable current velocity conditions to be converted into power density. This is only based on the trend of increasing velocity which increases from the bottom of the water to the surface.

Layers 4 and 5 with a depth variation of 3–4.5 meters were selected to assess the energy potential at station 1. The average velocity in this layer is 0.541–0.544 m/s, with a maximum speed of 1.033–1.04 m/s. Station 2 has a current velocity that can be utilized at layers 4 and 5 with a depth variation of 3–4 meters below the water surface. Each of the resulting average speeds of 0.329 m/s and 0.321 m/s, and a maximum of 0.626 m/s and 0.613 m/s. Station 3 has a current velocity that can be used in the conversion of power density is layer 5 and 6, the depth variation ranges from 2.5 to 4.0 meters. Each of the resulting average speeds of 0.275 m/s and 0.297 m/s, with a maximum current speed of 0.877 m/s and 0.904 m/s. Based on the vertical layer size of 0.5 meters, it is chosen for each station, two layers of depth with an estimated vertical layer size of 1m.

The layer near the bottom of the water is at a depth ranging from 6 to 5.5 meters at each station having a relatively smaller current velocity. The average current velocity is 0.460 m/s, 0.284 m/s and 0.304 m/s, respectively. The maximum speeds given are 0.890 m/s, 0.597 m/s, and 0.776 m/s. We will input this layer into each graph which is used as a comparison for the power density capacity generated at each station, with the previously selected layer.

Power density distribution at each depth layer

The distribution of power density at each depth varies greatly, this is related to each depth layer having a different current velocity due to interaction with the water layer below/above it, the surface layer, and the basic frictional force.

Tables 3, 4 and 5 show the variation of the average current velocity and average power density displayed in the analysis during the measurement for each station. Station 2 is shown in Table 4 with a ratio of 3 layers, including 2 selected layers and 1 bottom layer. The highest power density was found on April 11, 2021 with a power density value of 32,864 W/m² at layer 5, which is 1.4% different from layer 4 which has a power density of 32,374 W/m², and 34.1% different from layer 1 in the bottom layer of the waters.

Station 3 measurements on April 11–14, 2021. The highest value of the resulting power density is 75,157 W/m² at a depth of 3 meters. Compared to station 2 which is in the neap phase, it has a magnification of 56.3%. The 3.5-meter depth layer (layer 5) has a power density capacity of 64,188 W/m², this capacity differs slightly by 10,969 W/m².
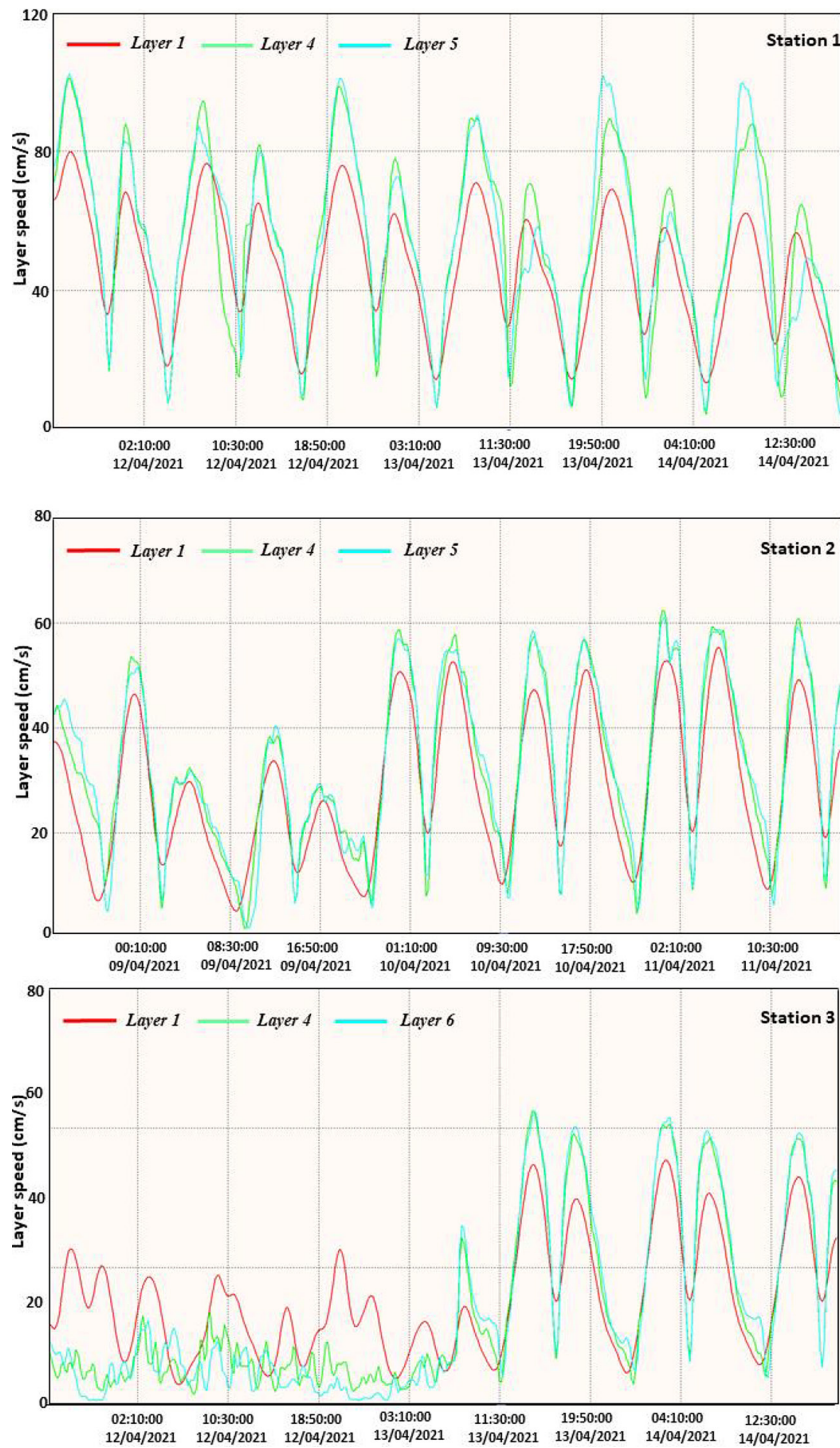
Figure 5. Current speed variation during ADCP measurement at three stations, comparing two selected layers and bottom layer

Station 1 measurements on the tide spring, this has optimized the presence of current velocity which is better utilized than the other two stations. The highest power density capacity is on April 14, 2021, at 235,344 W/m². Station 1 has a significantly high-power density capacity. Compared to station 3 on April 14, 2021 has the same tidal spring condition but station 1 is better in the converted power density capacity. Layer 4 at a depth of about 4 – 4.5 meters has a power density capacity of 221,874 W/m². The bottom layer of the water on the profile layer no 1 has a power density capacity of 128,399 W/m². The difference in power density capacity is due to the current velocity when the measurement at station 1 takes place during the full moon. Tidal current speed
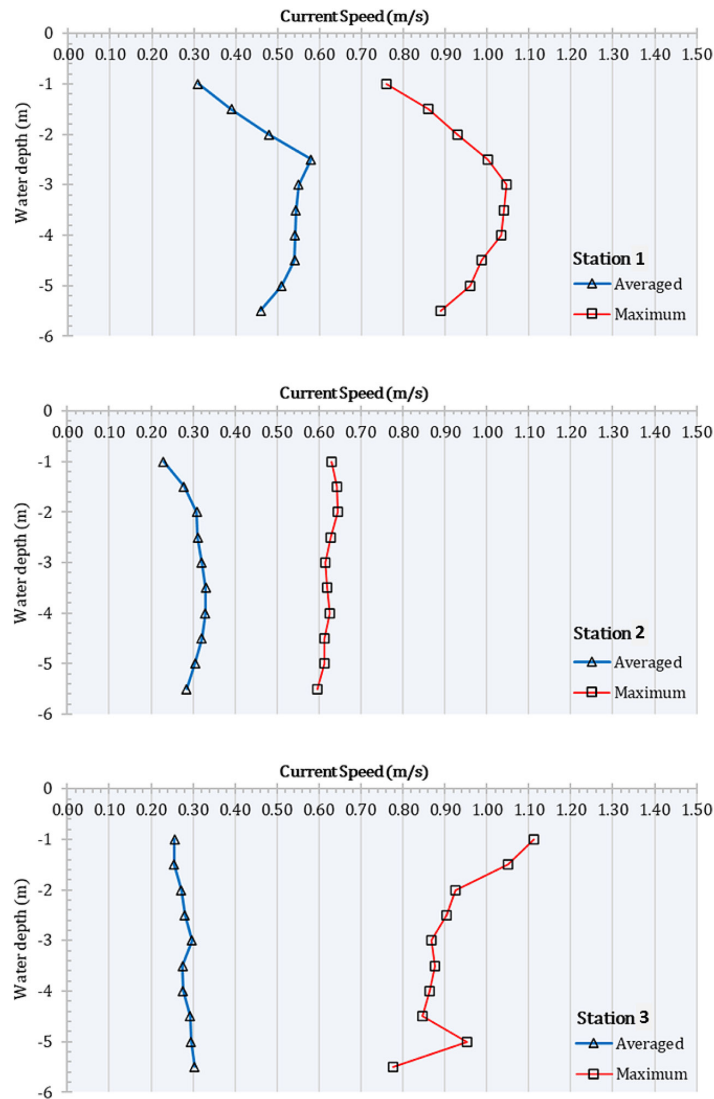
Figure 6. Current velocity profile derived from ADCP Station (Station 1–3), shown in the statistics of the average and maximum values, the top layer is below the LAT range

Table 3. Averaged power density estimation (W/m²) in depth layer (two selection layers and bottom layer) measured by ADCP all date at Station 1

Depth layer profile No.	Depth (m)	Current speed (m/s)				Power density (W/m²)			
		Apr-14	Apr-15	Apr-16	Apr-17	Apr-14	Apr-15	Apr-16	Apr-17
4	-4	0.756	0.563	0.533	0.455	221.874	91.636	77.754	48.370
5	-3.5	0.771	0.583	0.54	0.467	235.344	101.753	80.858	52.299
1	-5.5	0.63	0.499	0.449	0.383	128.399	63.803	46.481	28.849

Table 4. Averaged power density estimation (W/m²) in depth layer (two selection layers and bottom layer) measured by ADCP all date at Station 2

Depth layer profile No.	Depth (m)	Current speed (m/s)				Power density (W/m²)			
		Apr-08	Apr-09	Apr-10	Apr-11	Apr-08	Apr-09	Apr-10	Apr-11
4	-4	0.3297	0.235	0.369	0.398	18.403	6.664	25.800	32.374
5	-3.5	0.339	0.238	0.373	0.4	20.005	6.923	26.648	32.864
1	-5.5	0.256	0.211	0.322	0.348	8.615	4.824	17.144	21.641

Table 5. Averaged power density estimation (W/m²) in depth layer (two selection layers and bottom layer) measured by ADCP all date at Station 3

| Depth layer profile No.	Depth (m)	Current speed (m/s)				Power density (W/m²)			
		Apr-11	Apr-12	Apr-13	Apr-14	Apr-11	Apr-12	Apr-13	Apr-14
5	-3.5	0.087	0.101	0.322	0.5	0.338	0.529	17.144	64.188
6	-3	0.072	0.103	0.368	0.527	0.192	0.561	25.591	75.157
1	-5.5	0.337	0.22	0.282	0.431	19.653	5.468	11.516	41.112
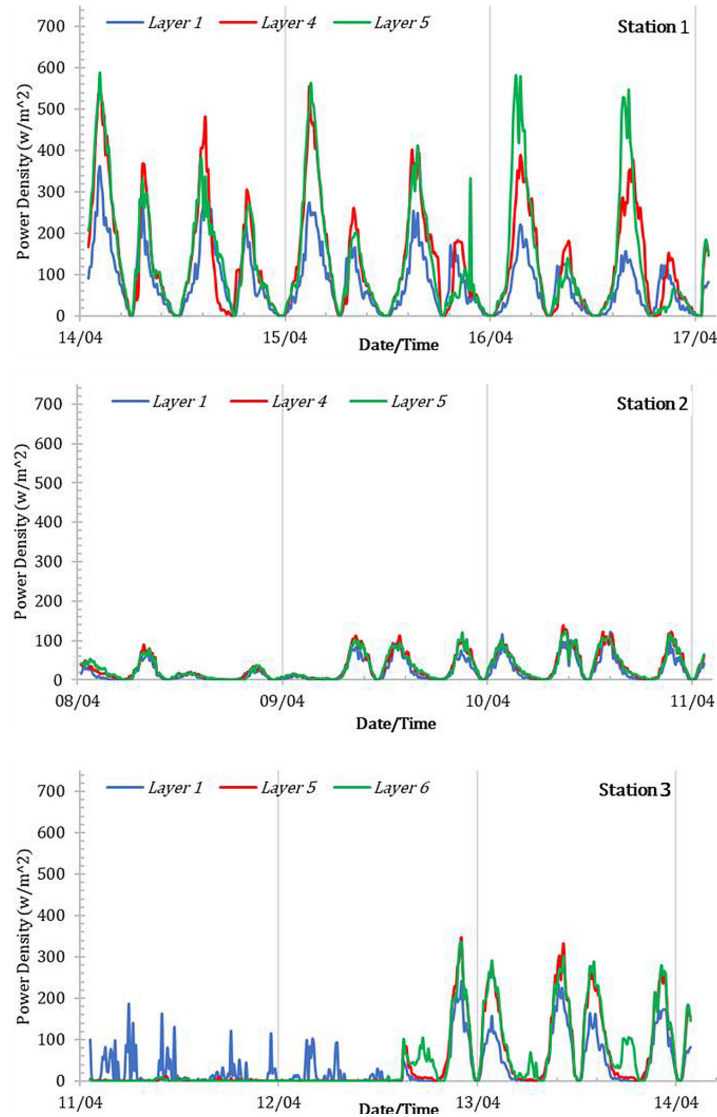
Fig. 7. Power density variation during ADCP measurement at 3 stations, comparing 2 selected layers and bottom layer

will increase and strengthen gradually significant when the full phase conditions are high, and the morphology is narrowed (Garcia Novo and Kyozuka, 2016; Kyozuka and Ogawa, 2006).

Figure 7, a graph showing the power density capacity during the measurement. This is done to make it easier to assess the daily fluctuations in power density at three different stations. Station

2 has a relatively smaller power density capacity ranging from 0 to 138,432 W/m². Layer 5 has a maximum power capacity that is converted from current speed of 122.3 W/m², Layer 4 is 138,432 W/m² and the most basic layer is 121,790 W/m². This maximum capacity appears with a time range of April 10–11, 2021. Stations 3 and 1 have a maximum power capacity of 346,369 W/m², 589,360
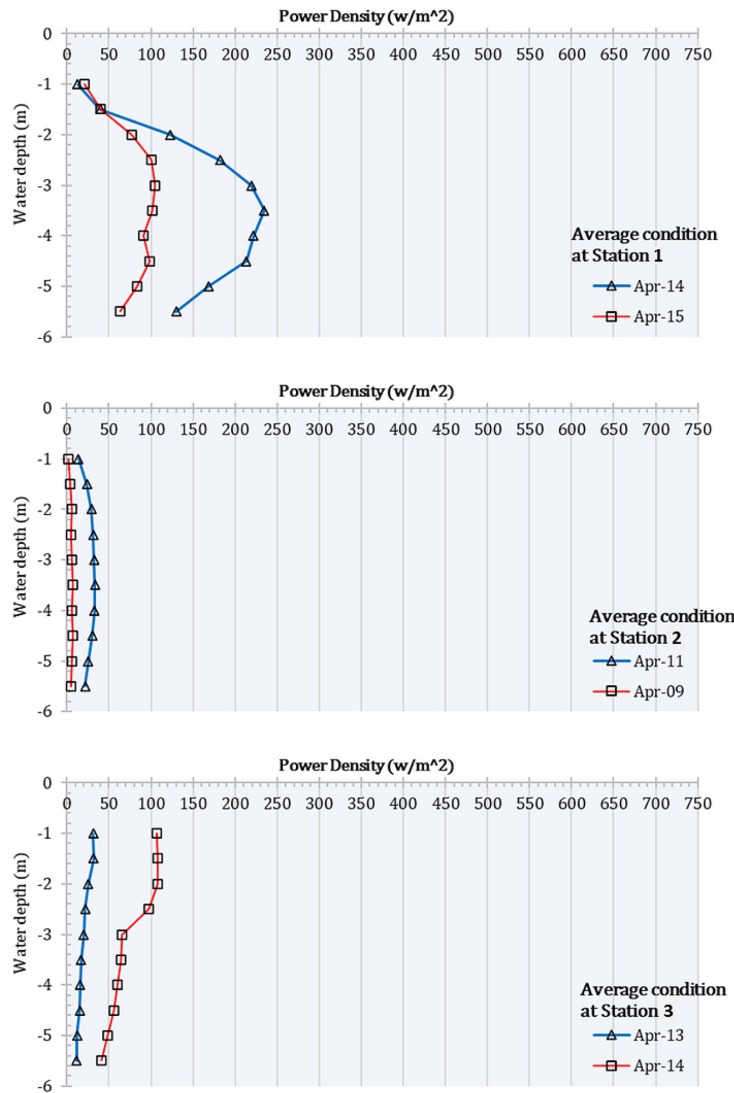
Figure 8. Averaged power density profile derived from current speed (Station 1–3), shown in the statistics of the average and maximum, comparing from two optimum date at each station

W/m² respectively. The difference in the maximum converted capacity between stations 3 and 1 is 242,991 W/m². Stations 3 and 1 have the potential to further develop the conversion of ocean currents into electrical energy due to measurements that take place during the daily spring to spring.

Station 1 has a good pattern during the measurement, it can be seen sinusoidally following the tides (El-Geziry and Couch, 2009; Siagian et al., 2021; Wei et al., 2016). Figure 6 shows the availability of optimal current capacity which can be converted into power density based on tidal riding. Using a cut in speed value of 0.5 m/s or the equivalent of 64.12 W/m², station 1 has a current capacity of 56.19% that can be utilized. This happens only during spring tide conditions. The distribution of power density capacity for the average of each depth for all stations is presented

in Figure 8. The distribution chosen is the power density from the date that has the optimal current velocity to be converted into power density. The power density at station 2 shows that April 11, 2021 vertically has a higher speed with a variation value of 13,726–33.11 W/m². Station 3 has a higher power density capacity on April 14, 2021 compared to the previous day. The distribution size from the layer near the base to the surface is 41.12 W/m², 48.052 W/m², 56,435 W/m², 59.676 W/m², 64.118 W/m², 64,961 W/m², 97.113 W/m², 107.62 W/m², 108.17 W/m², and 106,538 W/m².

Station 1 shows a trend of higher power density capacity compared to other stations. Power density capacity on April 14, 2021 with a range of 12,850–234,430 W/m². However, the current speed value has a power density capacity that can be electrified, not all can be extracted, only values

above the cut in speed can be electrified. The selection of optimal water depths and the selection of turbines that have a smaller cut in speed value will help the development of electrification be carried out better (Hagerman and Polagye, 2006).

CONCLUSIONS

We have carried out measurements at three different stations with the same length of time for each station. Based on the results of current velocity measurements that can be used as renewable energy, it is found at station 2 with a depth of 3.5 meters and a current speed of 0.4 m/s with a power density value of 32.86 W/m². Station 3 is located at a depth of 3 meters with a current speed of 0.527 m/s with a power density value of 75,157 W/m². Station 1 is located at a depth of 4 meters with a current speed of 235,344 W/m². Station 1 is the location that has the highest power density capacity, this is related to the measurement time during tidal spring.

REFERENCES

1. Abbaspour, M., Rahimi, R. 2011. Iran atlas of offshore renewable energies. Renewable Energy 36, 388–398. https://doi.org/10.1016/j.renene.2010.06.051

2. Aroussy, Y., Nachtane, M., Saifaoui, D., Tarfaoui, M. 2016. Numerical investigation of a reverse osmosis desalination system with cogeneration and renewable energy... Numerical investigation of a reverse osmosis desalination system with cogeneration and renewable energy integration.

3. Blunden, L.S., Bahaj, A.S. 2006. Initial evaluation of tidal stream energy resources at Portland Bill, UK. Renewable Energy 31, 121–132. https://doi.org/10.1016/j.renene.2005.08.016

4. Bouchkara, M., El Khalidi, K., Benazzouz, A., Erraji Chahid, N., Joudar, I., Zourarah, B., Maanan, M. 2022. Study of morphodynamic and sedimentological changes in the oualidia lagoon (morocco) using bathymetric data: first investigations after the sediment trap dredging. The International Archives of the Photogrammetry, Remote Sensing and Spatial Information Sciences XLVI-4/W3-2021, 53–63. https://doi.org/10.5194/isprs-archives-XLVI-4-W3-2021-53-2022

5. Cornett, A., Durand, N., Bourban, S. 2010. 3D Modelling and Assessment of Tidal Current Energy Resources in the Bay of Fundy. Proceedings of the 3rd International Conference on Ocean Energy, 2–7.

6. Cowles, G.W., Hakim, A.R., Churchill, J.H. 2017. A comparison of numerical and analytical predictions of the tidal stream power resource of Massachusetts, USA. Renewable Energy, 114, 215–228. https://doi.org/10.1016/j.renene.2017.05.003

7. El-Geziry, T.M., Couch, S.J. 2009. Environmental impact assessment for tidal energy schemes: An exemplar case study of the Strait of Messina. Proceedings of the Institute of Marine Engineering, Science and Technology Part A: Journal of Marine Engineering and Technology, 4177, 39–48. https://doi.org/10.1080/20464177.2009.11020217

8. El Khalidi, K., Zourarah, B., Aajjane, A. 2011. Evolution récente de la morphologie de delta de flot et son effet sur la dynamique hydro-sédimentaire de la lagune de Oualidia (côte atlantique, Maroc): approche par photographie aérienne. Estudos do Quaternário, 7, 73–78.

9. Ferro, B. 2006. Wave and Tidal Energy: Its Emergence and the Challenges it Faces. Refocus, 7(3), 46–48.

10. Garcia Novo, P., Kyozuka, Y. 2016. Field measurement and numerical study of tidal current turbulence intensity in the Kobe Strait of the Goto Islands, Nagasaki Prefecture. Journal of Marine Science and Technology. https://doi.org/10.1007/s00773-016-0414-x

11. Geme, 2003. Diagnosis and studies of the containment of the Oualidia lagoon - Phase 2 - Measurement campaign. Royaume du Maroc : Direction Provinciale de l'Equipement d'El Jadida, Ministère de l'Equipement et du Transport, 60.

12. Guillou, N., Neill, S.P., Robins, P.E. 2018. Characterising the tidal stream power resource around France using a high-resolution harmonic database. Renewable Energy, 123, 706–718. https://doi.org/10.1016/j.renene.2017.12.033

13. Hagerman, G., Polagye, B. 2006. Methodology for estimating tidal current energy resources and power production by tidal in-stream energy conversion (TISEC) devices. Electric Power Research Institute.

14. Hilmi, K., Orbi, A., Lakhdar, J.I., Sarf, F. 2005. Etude courantologique de la lagune de Oualidia (Maroc) en automne, 7, 67–71.

15. Iglesias, G., Carballo, R. 2014. Wave farm impact: The role of farm-to-coast distance. Renewable Energy, 69, 375–385. https://doi.org/10.1016/j.renene.2014.03.059

16. Ismanto, A., Ismunarti, D.H., Sugianto, D.N., Maisyarah, S., Subardjo, P., Dwi Suryoputro, A.A., Siagian, H. 2019. The potential of ocean current as electrical power sources alternatives in Karimunjawa Islands Indonesia. Advances in Science, Technology and Engineering Systems, 4, 126–133. https://doi.

org/10.25046/aj040615

17. Karim, H., Omar, E., Mohammed, I., Jamila, L., Benyounes, A., Zineb, E., Abdellatif., etOrbi, Ahmed, M. 2017. Fonctionnement Hydrodynamique De La Lagune De Oualidia (Maroc) Avant L'Amenagement De La Souille. International Journal of Advanced Research, 5, 2015–2027. https://doi.org/10.21474/ijar01/4937

18. Kiho, B. 2011. Tests on Ducted and Bare helical and straight blade Darrieus hydrokinetic turbines, Renewables Energy, 36, 3013–3022.

19. Koutitonsky, V.G., Orbi, A., Ouabi, M. et I.I., n.d. L'étude du comportement hydro-sédimentaire du système lagunaire Oualidia par la modélisation mathématique. Phase 1 : Synthèse des données et simulations de la réfraction des houles. Direction des Ports et du Domaine Public Maritime, Ministère de l'Équipement et du Transport, Royaume du Maroc, 150.

20. Koutitonsky, V.G., Ouabi, M., I.I. 2007. L'étude du comportement hydrosédimentaire du système lagunaire Oualidia par la modélisation mathématique. Phase 2: Modélisation hydro-sédimentaire de l'état actuel et de scenarios d'aménagement. Direction des Ports et du Domaine Public Maritime, Ministère de l'Équipement et du Transport, Royaume du Maroc 204 p + Annexes, 40.

21. Kyozuka, Y., Ogawa, K. 2006. Tidal Current Power Generation Making Use of a Bridge Pier. OCEANS 2006 - Asia Pacific 1–8. https://doi.org/10.1109/OCEANSAP.2006.4393925

22. L'Electricité, O.N. de. 2020. Global Rural Electrification Program (PERG). Rapport Annuel. Morocco: ONE.

23. Mejia-Olivares, C.J., Haigh, I.D., Wells, N.C., Coles, D.S., Lewis, M.J., Neill, S.P. 2018. Tidal-stream energy resource characterization for the Gulf of California, México. Energy, 156, 481–491. https://doi.org/10.1016/j.energy.2018.04.074

24. MEMEE. 2012. Les Energies Renouvelables au Maroc: Stratégie et plan d'action. Ministère de l'Energie, des Mines, de l'Eau et de l'Environnement (MEMEE).

25. Moreno N., et. al. 2010. Ocean Current's Energy: How to produce electrical energy thanks to the marine currents. Report of Renewable Energy Project 2008, Hogskolan I Gavle.

26. Neill, S.P., Angeloudis, A., Robins, P.E., Walkington, I., Ward, S.L., Masters, I., Lewis, M.J., Piano, M., Avdis, A., Piggott, M.D., Aggidis, G., Evans, P., Adcock, T.A.A., Židonis, A., Ahmadian, R., Falconer, R. 2018. Tidal range energy resource and optimization – Past perspectives and future challenges. Renewable Energy, 127, 763–778. https://doi.org/10.1016/j.renene.2018.05.007

27. Pu, X., Shi, J.Z., Hu, G.D. 2017. The effect of stratification on the vertical structure of the tidal ellipse in the Changjiang River estuary, China. Journal of Hydro-Environment Research, 15, 75–94. https://doi.org/10.1016/j.jher.2017.03.004

28. Ren, L., Nash, S., Hartnett, M. 2015. Observation and modeling of tide- and wind-induced surface currents in Galway Bay. Water Science and Engineering, 8, 345–352. https://doi.org/10.1016/j.wse.2015.12.001

29. Rourke, F.O., Boyle, F., Reynolds, A. 2010. Marine current energy devices: Current status and possible future applications in Ireland. Renewable and Sustainable Energy Reviews, 14, 1026–1036. https://doi.org/10.1016/j.rser.2009.11.012

30. Rusu, L., Onea, F. 2015. Assessment of the performances of various wave energy converters along the European continental coasts. Energy, 82, 889–904. https://doi.org/10.1016/j.energy.2015.01.099

31. Serhadlıoğlu, S., Adcock, T.A.A., Houlsby, G.T., Draper, S., Borthwick, A.G.L. 2013. Tidal stream energy resource assessment of the Anglesey Skerries. International Journal of Marine Energy, 3–4, e98–e111. https://doi.org/10.1016/j.ijome.2013.11.014

32. Siagian, H., Ismanto, A., Putra, T.W.L., Pranata, 2021. Stratification on the Vertical Structure of the Tidal Ellipse and Power Density Estimation in the Larantuka Strait, East Flores Based on ADCP Measurement Data. IOP Conference Series: Earth and Environmental Science, 750, 012023. https://doi.org/10.1088/1755-1315/750/1/012023

33. Siagian, H., Sugianto, D., Kunarso. 2019a. Current Velocity Impacts from Interaction of Semidiurnal and Diurnal Tidal Constituents for Tidal Stream Energy in East Flores Current Velocity Impacts from Interaction of Semidiurnal and Diurnal Tidal Constituents for Tidal Stream Energy in. IOP Conference Series: Earth and Environmental Science, 246, 246. https://doi.org/10.1088/1755-1315/246/1/012056

34. Siagian, H., Sugianto, D.N., Kunarso, Pranata, A.S. 2019b. Estimation of Potential Energy Generated From Tidal Stream in Different Depth Layer at East Flores Waters Measured by ADCP. IOP Conference Series: Earth and Environmental Science, 246, 12052. https://doi.org/10.1088/1755-1315/246/1/012052

35. Sierra, J.P., González-Marco, D., Sospedra, J., Gironella, X., Mösso, C., Sánchez-Arcilla, A. 2013. Wave energy resource assessment in Lanzarote (Spain). Renewable Energy, 55, 480–489. https://doi.org/10.1016/j.renene.2013.01.004

36. Togneri, M., Lewis, M., Neill, S., Masters, I. 2017. Comparison of ADCP observations and 3D model simulations of turbulence at a tidal energy site. Renewable Energy, 114, 273–282. https://doi.org/10.1016/j.renene.2017.03.061

37. Wei, Z., Fang, G., Susanto, R.D., Adi, T.R., Fan, B., Setiawan, A., Li, S., Wang, Y., Gao, X. 2016. Tidal elevation, current, and energy flux in the area between the South China Sea and Java Sea. Ocean Science, 12, 517–531. https://doi.org/10.5194/os-12-517-2016